SUPPORTING INFORMATION

Membrane Binding of Recoverin: From Mechanistic Understanding to Biological Functionality

Štěpán Timr, Roman Pleskot, Jan Kadlec, Miriam Kohagen, Aniket Magarkar,

and Pavel Jungwirth

Table S1. Overview of recoverin–membrane atomistic simulations. In run 1, recoverin approached the lipid bilayer with the C-terminus, which brought the myristoyl anchor in a position away from the membrane. This orientation persisted for the entire duration of the simulation. In run 2, no membrane insertion of myristoyl occurred despite a favorable orientation of recoverin toward the membrane since the myristoyl group became sequestered in between amino acid side chains. Recoverin became successfully membrane-anchored in run 3, as shown in Figure 2 of the main text. In runs 4–6, it approached the lipid bilayer with the C-terminus. Membrane insertion of the myristoyl moiety was also observed with the AMBER force field, as documented by runs 7 and 9. In run 8, no myristoyl insertion occurred as helix A lost its secondary structure in the course of the simulation and the myristoyl moiety moved to the binding site for rhodopsin kinase. In run 10, recoverin interacted with the lipid bilayer via the C-terminus. In runs 11–15, no myristoyl insertion was observed as the myristoyl group was sequestered from the aqueous environment. In contrast, binding of rhodopsin kinase (runs 16–18) prevented the myristoyl moiety from moving in between amino acid side chains, allowing for its successful membrane insertion. Runs 19–21 without the C-terminal segment eliminated the unfavorable orientation which moved the myristoyl anchor away from the membrane, but at the same time, in runs 19 and 21 removal of the C-terminus altered the conformation of the protein. Finally, in run 22, continued from run 3 after deletion of the myristoyl moiety, recoverin detached from the membrane.

Run	Membrane	Force field	Trajectory length [ns]	Myristoyl exposed	Myristoyl insertion	Comments
1	PC:PG (4:1)	CHARMM	710	NO	NO	Fig. S5
2	PC:PG (4:1)	CHARMM	530	NO	NO	
3	**PC:PG (4:1)**	**CHARMM**	**1000**	**YES**	**YES**	Figs. 2, S1, S2
4	PC:PG (4:1)	CHARMM	180	YES	NO	
5	PC:PG (4:1)	CHARMM	120	YES	NO	
6	PC:PG (4:1)	CHARMM	120	YES	NO	
7	**PC:PG (4:1)**	**AMBER**	**1000**	**YES**	**YES**	Figs. S1, S2, S8 and S10
8	PC:PG (4:1)	AMBER	320	NO	NO	
9	**PC:PG (4:1)**	**AMBER**	**460**	**YES**	**YES**	Fig. S1
10	PC:PG (4:1)	AMBER	200	NO	NO	Fig. S8
11	PG	AMBER	1000	NO	NO	

Table S1 (continuation). Overview of recoverin–membrane atomistic simulations.

Run	Membrane	Force field	Trajectory length [ns]	Myristoyl exposed	Myristoyl insertion	Comments
12	PG	AMBER	330	NO	NO	
13	PG	AMBER	670	NO	NO	
14	PG	AMBER	2000	NO	NO	Fig. S6
15	PC	AMBER	360	NO	NO	
16	**PC:PG (4:1)**	**AMBER**	**500**	**YES**	**YES**	With a fragment of rhodopsin kinase, Figs. S1, S9
17	**PC:PG (4:1)**	**AMBER**	**320**	**YES**	**YES**	With a fragment of rhodopsin kinase
18	**PC:PG (4:1)**	**AMBER**	**320**	**YES**	**YES**	With a fragment of rhodopsin kinase
19	PC:PG (4:1)	CHARMM	240	YES	NO	Without C-terminal residues 190─202
20	PC:PG (4:1)	CHARMM	420	YES	NO	Without C-terminal residues 190─202
21	PC:PG (4:1)	CHARMM	240	YES	NO	Without C-terminal residues 190─202
22	PC:PG (4:1)	CHARMM	250	-	-	Without myristoyl moiety; Fig. S3

Table S2. Overview of recoverin–membrane coarse-grained simulations. NONPOL refers to the standard non-polarizable MARTINI model while POL denotes the polarizable version of MARTINI (see Supporting Methods). Myristoyl insertion was observed irrespective of the membrane composition.

Run	Membrane	Force field	Trajectory length [μs]	Myristoyl exposed	Myristoyl insertion
1	PC	NONPOL	5	YES	NO
2	PC	NONPOL	5	YES	YES
3	PC	NONPOL	5	YES	YES
4	PC:PG (4:1)	NONPOL	5	YES	YES
5	PC:PG (4:1)	NONPOL	5	YES	YES
6	PC:PG (4:1)	NONPOL	5	YES	YES
7	PG	NONPOL	5	YES	YES
8	PG	NONPOL	5	YES	YES
9	PG	NONPOL	5	YES	YES
10	PC:PG (4:1)	POL	2.5	YES	YES
11	PC:PG (4:1)	POL	2.5	YES	YES
12	PC:PG (4:1)	POL	2.5	YES	YES

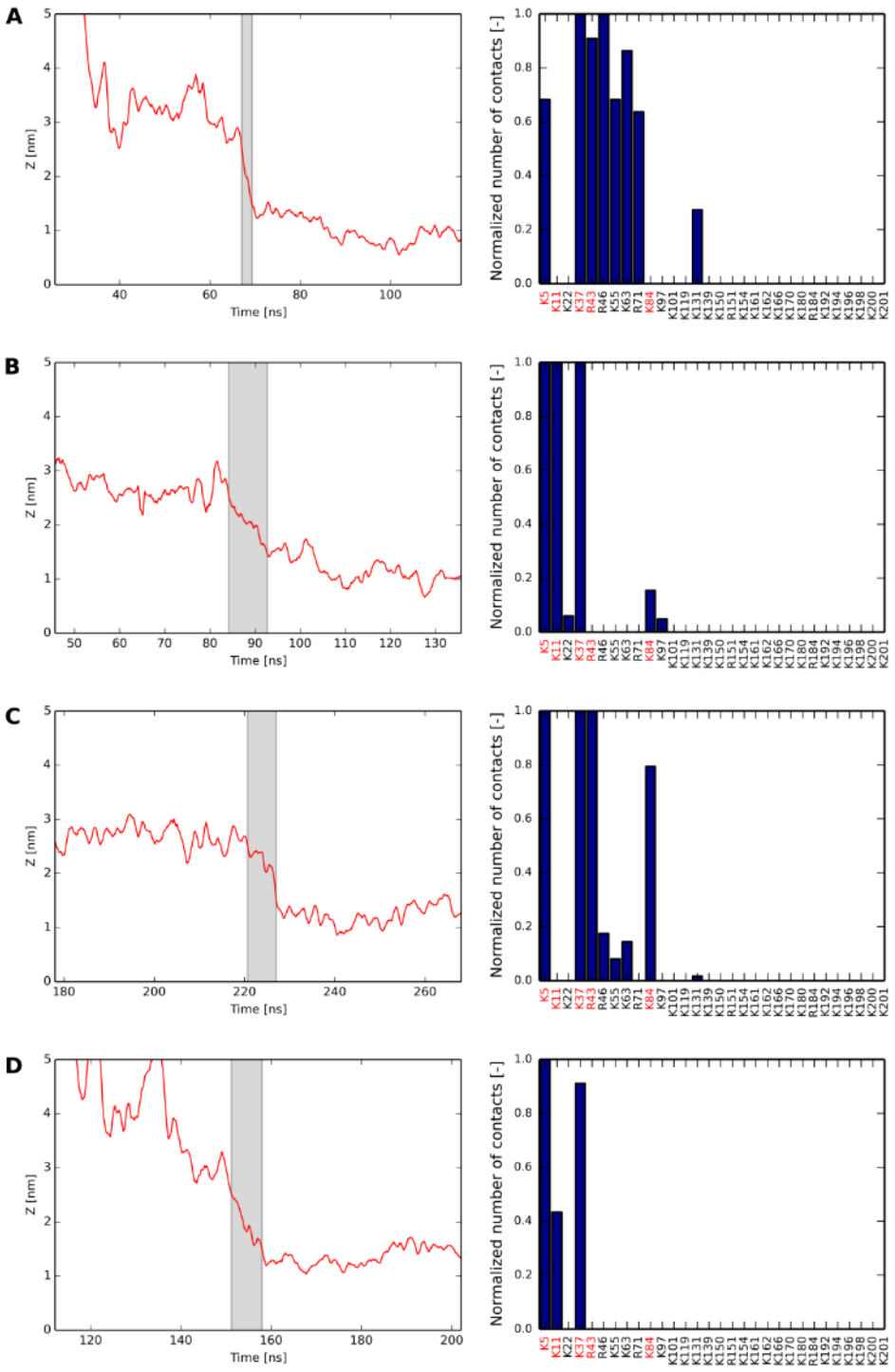

Figure S1. The process of myristoyl insertion: The distance *z* of the methyl end of the myristoyl moiety from the central plane of the bilayer (left) with the time interval where *z* is between 2.5 and 1.5 nm shown in gray, and the membrane contacts of different basic amino acid residues during this time interval (right). (A) run 3, (B) run 7, (C) run 9, (D) run 16. The time needed for myristoyl insertion varied between 2 and 9 ns.

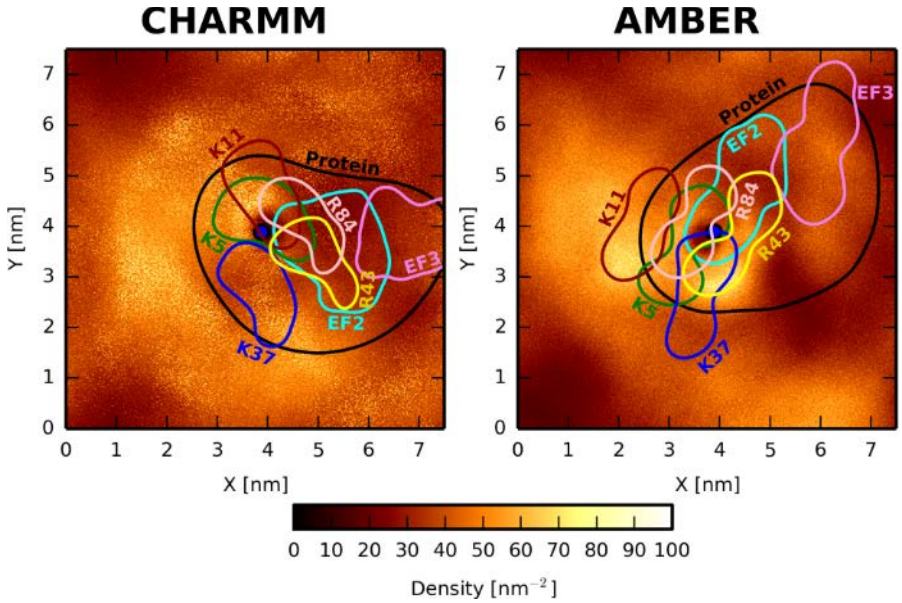

Figure S2. Density maps of negatively charged PG lipids in the membrane leaflet proximal to recoverin. Results from two PC:PG (4:1) simulations featuring insertion of the myristoyl moiety to the bilayer: run 3 (left) and run 7 (right). The density maps are centered on the myristoyl group (blue dot in the middle); the contours indicate the positions of the protein as well as those of several charged amino acid residues and the two calcium ions.

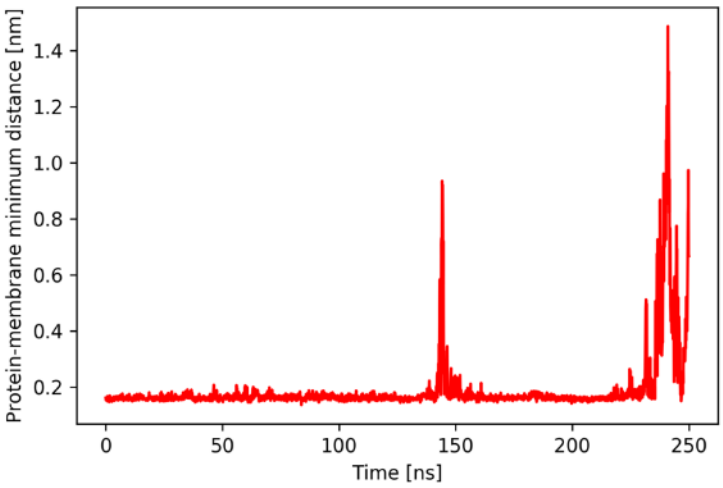

Figure S3. Myristoyl moiety is crucial for stable membrane binding of recoverin. The plot shows the minimum distance between recoverin and membrane surface in a simulation (run 22) started from the final snapshot of run 3 (i.e., PC:PG (4:1) membrane, CHARMM force field, spontaneous insertion) after removal of the myristoyl group. The orientation of recoverin relative to the membrane became destabilized, and ultimately, recoverin detached itself completely from the membrane surface (~240 ns). After the detachment, recoverin rotated and approached the membrane with its C-terminus. Since some of our simulations showed that this mode of interaction is difficult to escape in all-atom MD, we decided to terminate the run at this point. It is important to note that our coarse-grained simulations indicate that the interaction via the C-terminus only represents a local minimum, and therefore, it is by itself not sufficient for stable membrane binding.

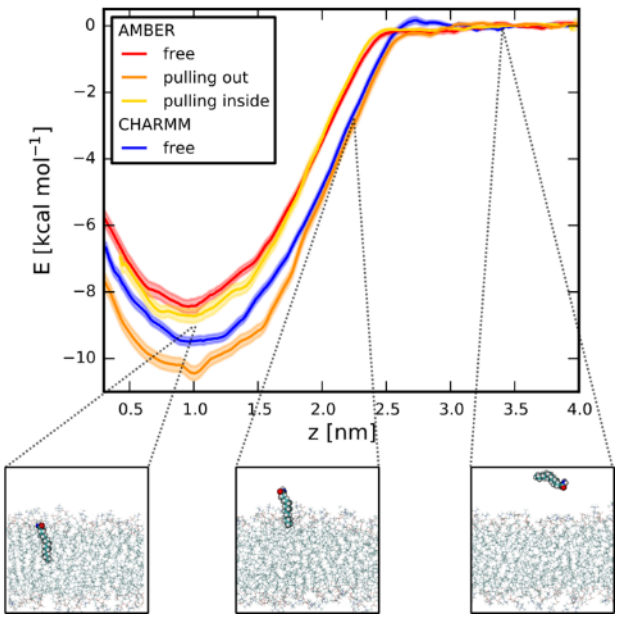

Figure S4. Free energy profiles of myristamide insertion into a PC:PG (4:1) membrane: A comparison of the CHARMM and AMBER/Slipids force fields and of different choices of the initial geometries. The starting geometries for individual umbrella windows were generated from spontaneous myristamide insertions observed in direct MD simulations (free) or from its harmonic restraint pulling inside or outside the bilayer (see Supporting Methods for more details).

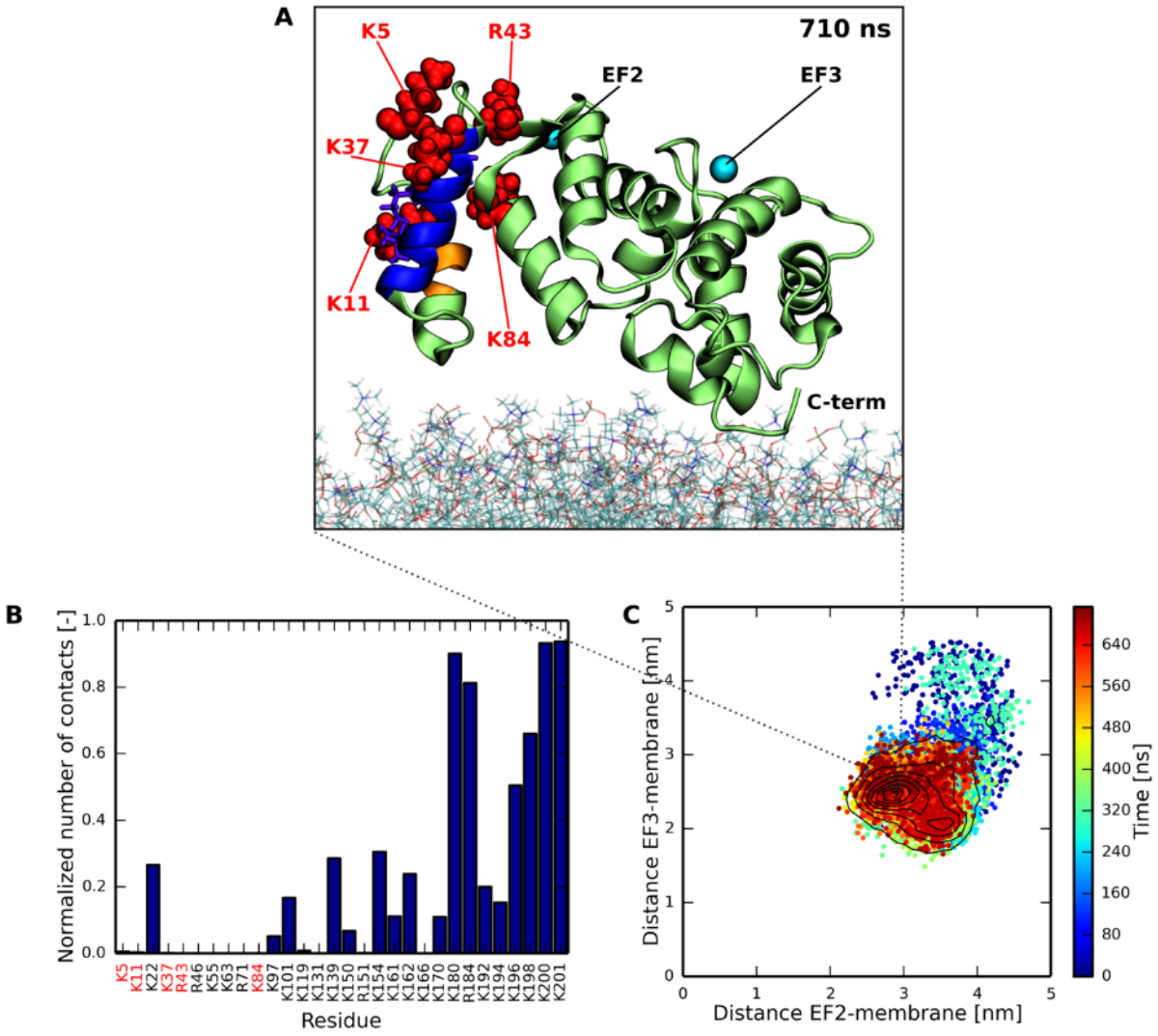

Figure S5. Results from a simulation of recoverin in the proximity of a PC:PG (4:1) bilayer (run 1), where the positively charged C-terminus of recoverin interacted heavily with the membrane. (A) Snapshot obtained at the end of the trajectory showing five basic protein residues (red) reported by previous NMR experiments [1] to be in close contact with the membrane. (B) Fraction of simulation time that each basic protein residue spent in contact with the bilayer (distance < 0.6 nm). The five residues from NMR are highlighted in red. (C) Evolution of the membrane orientation of recoverin in the course of the trajectory. The orientation is expressed in terms of the membrane distances of the two calcium ions.

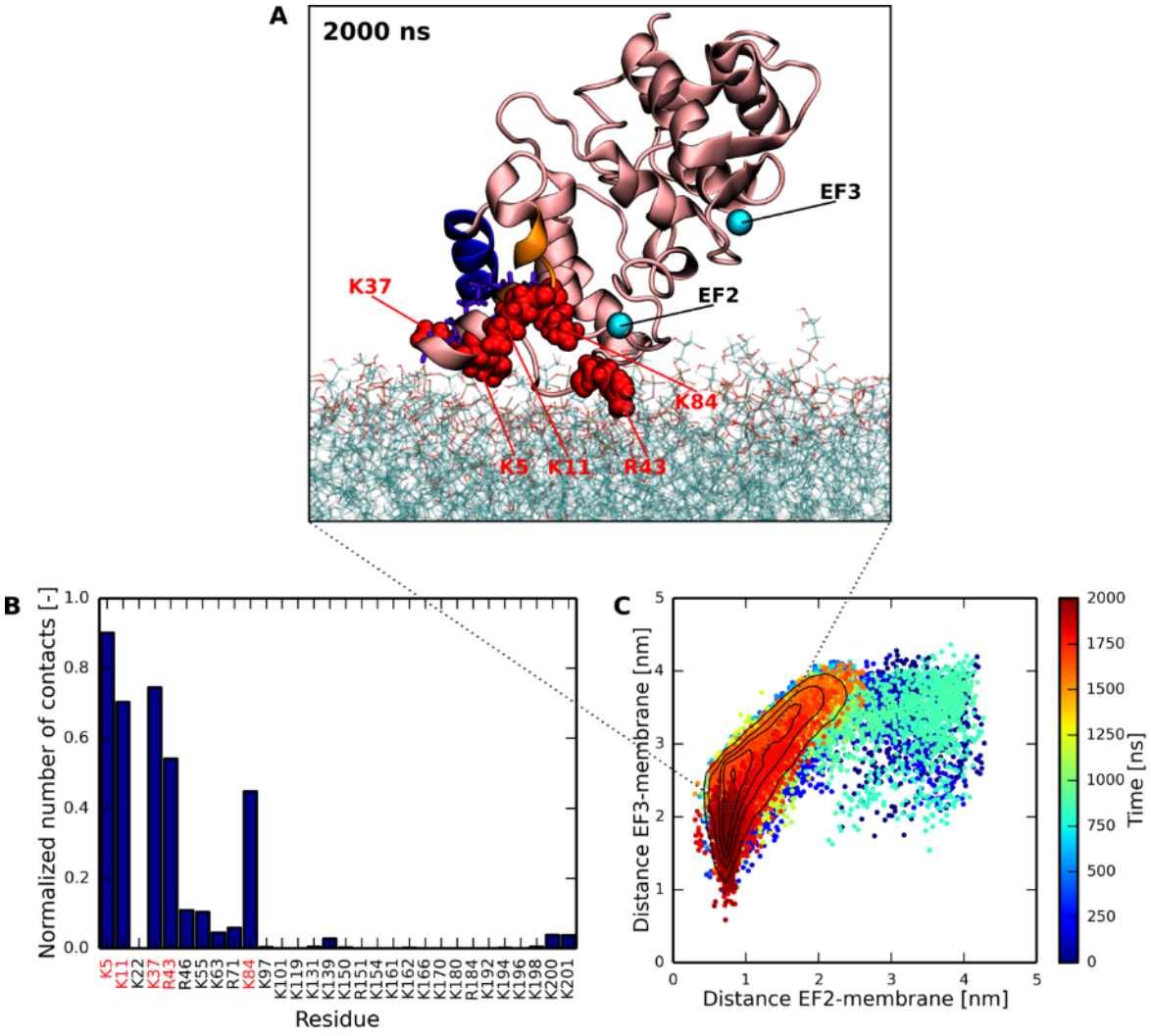

Figure S6. Results from a simulation of recoverin in the proximity of a PG bilayer (run 14). Here the protein adopted a tilted orientation relative to the membrane. (A) Snapshot obtained at the end of the trajectory showing five basic protein residues (red) reported by previous NMR experiments[1] to be in close contact with the membrane. (B) Fraction of simulation time that each basic protein residue spent in contact with the bilayer (distance < 0.6 nm). The five residues from NMR are highlighted in red. (C) Evolution of the membrane orientation of recoverin in the course of the trajectory. The orientation is expressed in terms of the membrane distances of the two calcium ions.

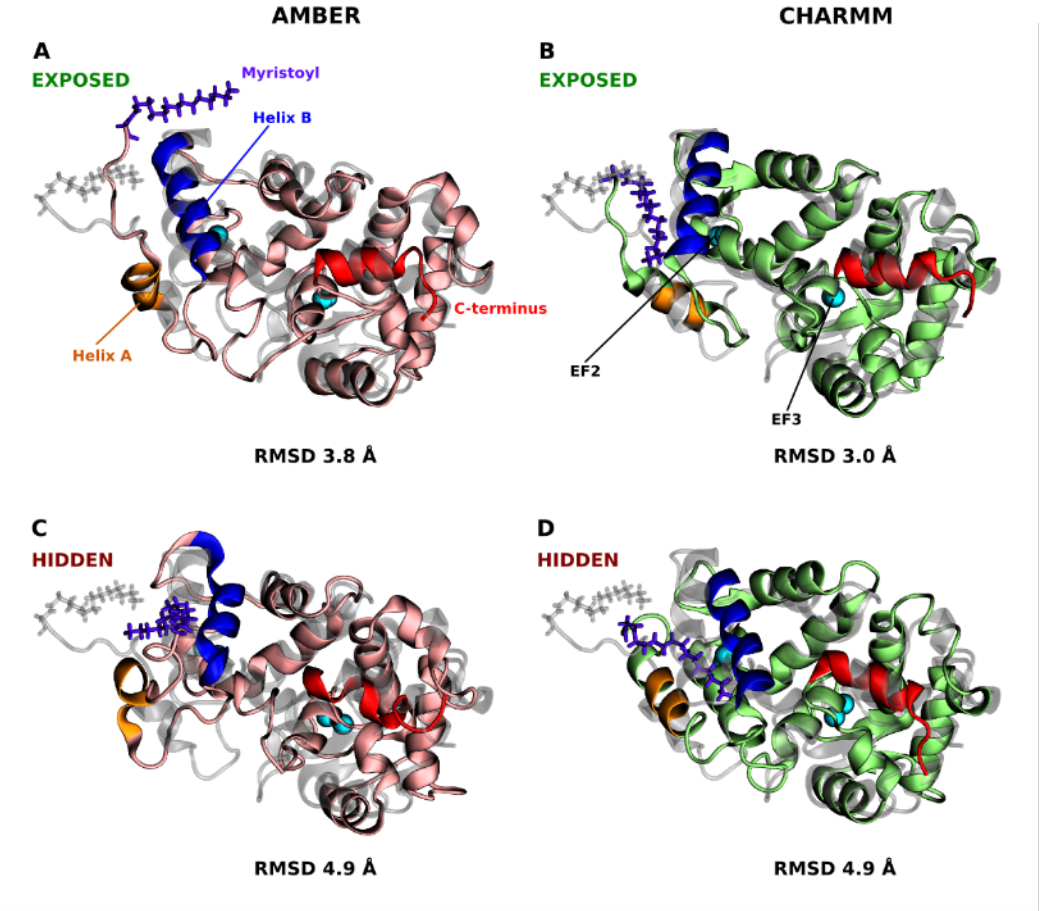

Figure S7. Examples of recoverin structures obtained after a 100 ns simulation in a 150 mM KCl solution following equilibration. Initial geometries and equilibration protocols: (A) 1JSA 8, protocol 2, (B) 1JSA 1, protocol 1, (C) 1JSA 1, protocol 1, (D) 1JSA 1, protocol 2. (for details see Supporting Methods and Table S6). The choice of the initial geometry from the ensemble of structures determined by NMR, the choice of the force field, or the details of the equilibration protocol could have an effect on the stability of the N-terminal domain and on the ability of the myristoyl moiety to anchor recoverin in the lipid bilayer. Therefore, to investigate potential effects of these factors, we relaxed the structure using two different starting geometries from NMR (structures 1 and 8 from PDB 1JSA), two different force fields CHARMM22/CMAP[2-3] and AMBER ff99SB-ILDN,[4] together with two different equilibration protocols (see Supporting Methods for details). We found that after a 100 ns unrestrained simulation following equilibration, all but two combinations of the initial structure, force field, and equilibration protocol led to changes in the conformation of helices A and B and, in turn, to sequestration of the myristoyl group from the aqueous environment (see also Table S6). While in the simulations with the AMBER force field helix A was generally prone to losing its secondary structure, it had a tendency to become longer in the CHARMM simulations and, at the same time, more parallel with helix B. Irrespective of the force field used, the motion of helix B continued narrowing the RK binding pocket. In contrast, the two cases with the myristoyl group exposed, which were obtained with exactly the opposite choices of the structure, force field, and equilibration protocol, exhibited smaller RMSDs with respect to the starting structures, and the angles between helices A and B remained close to perpendicular.

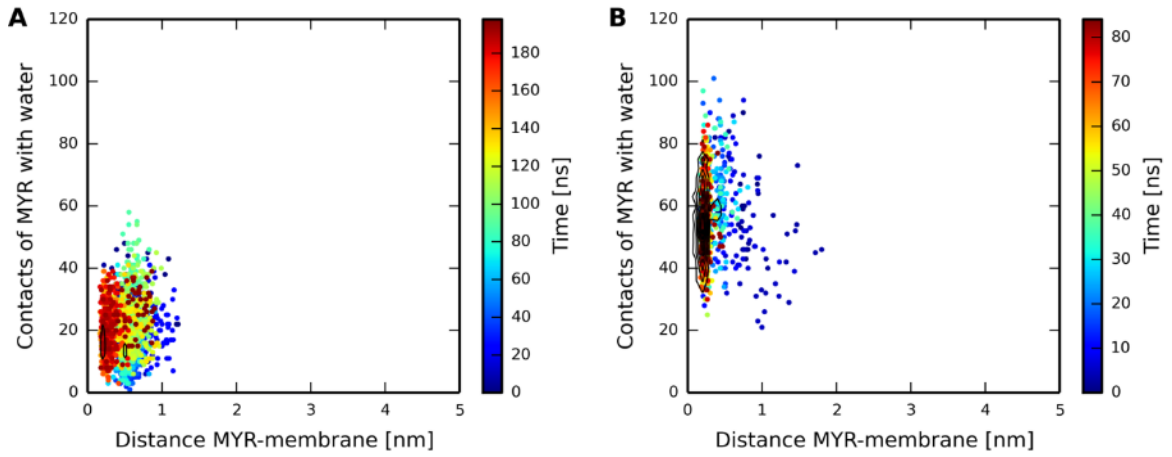

Figure S8. Exposure of myristoyl to water is critical for its successful membrane insertion. (A) Trajectory without membrane insertion of the myristoyl moiety (run 10), and (B) a trajectory with successful myristoyl insertion (run 7), before the insertion event. The plots show the number of contacts (distance < 0.3 nm) of the myristoyl moiety with water molecules plotted against the distance of the myristoyl group from the membrane surface.

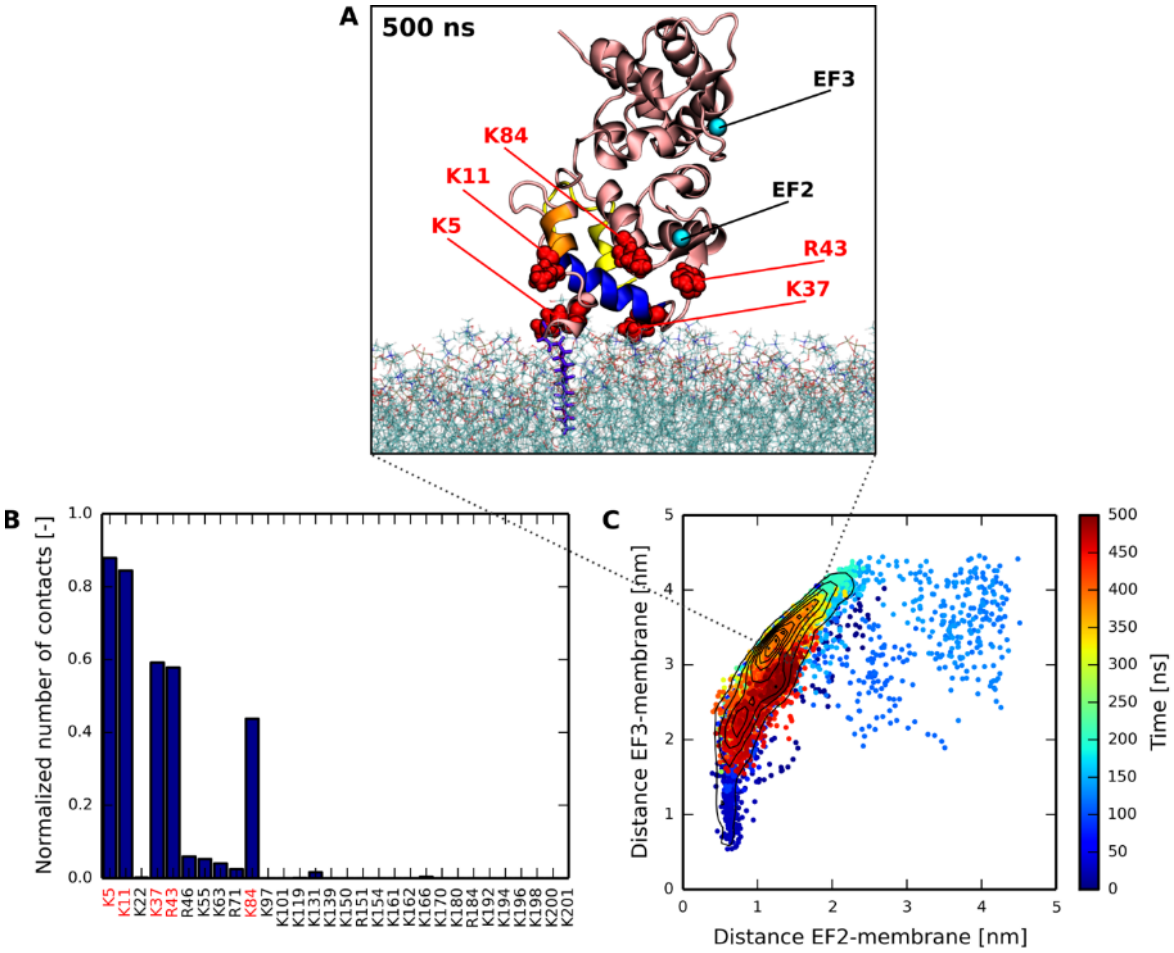

Figure S9. The myristoyl group of recoverin binding a fragment of rhodopsin kinase (RK) is capable of insertion into a PC:PG (4:1) membrane. The RK fragment increased the conformational stability of the N-terminal domain, with the Cα root-mean-square deviation of residues 2–97 (N-terminal domain) from the initial NMR structure equaling 0.31 nm, as contrasted to 0.48 nm in run 10 without RK. (A) Snapshot from the end of a 500 ns trajectory (run 16) showing the membrane-embedded myristoyl moiety (violet) and five positively charged residues (red) reported by previous NMR experiments[1] to interact with the membrane. (B) Fraction of simulation time that each positively charged residue of recoverin spent in contact with the membrane (distance < 0.6 nm). The five residues from NMR are highlighted in red. (C) Evolution of the membrane orientation of recoverin in the course of the 500 ns trajectory. The orientation is expressed in terms of the membrane distances of the two calcium ions, and the most populated area corresponds to a tilted orientation with the EF2-bound calcium closer to the bilayer and EF3-bound calcium farther away.

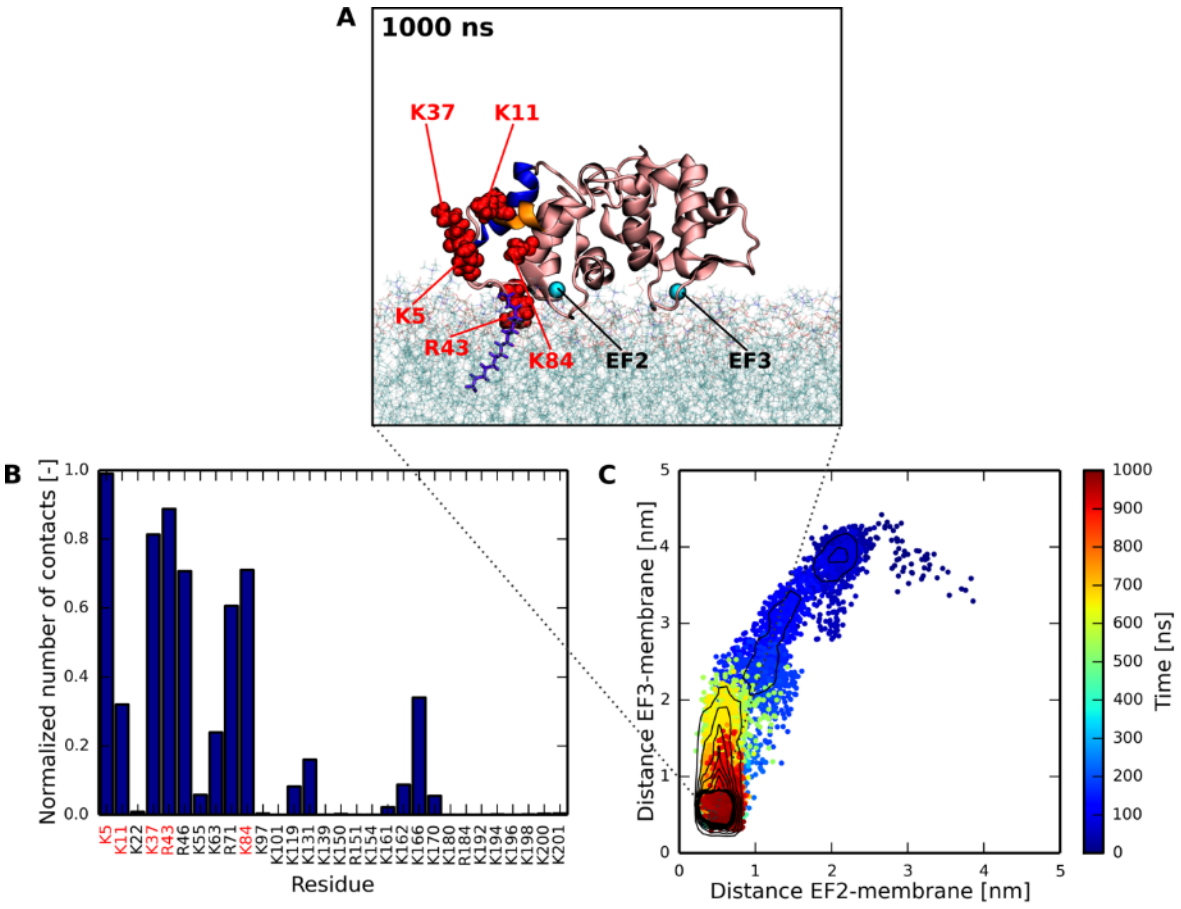

Figure S10. Recoverin with an exposed myristoyl group becomes anchored in a PC:PG (4:1) membrane (run 7, AMBER force field). (A) Snapshot from the end of a 1000 ns trajectory, featuring the membrane-inserted myristoyl group (violet) and five positively charged residues (red) known from previous NMR measurements[1] to interact with the membrane. (B) Relative proportion of simulation time that each basic residue of recoverin spent in contact with the membrane (distance < 0.6 nm). (C) Membrane orientation of recoverin during the 1000 ns trajectory described in terms of the membrane distances of the two calcium ions. The prevalent orientation was parallel to the membrane, with both calcium ions in a close proximity to the membrane surface. The binding pocket for rhodopsin kinase remained accessible throughout the entire trajectory.

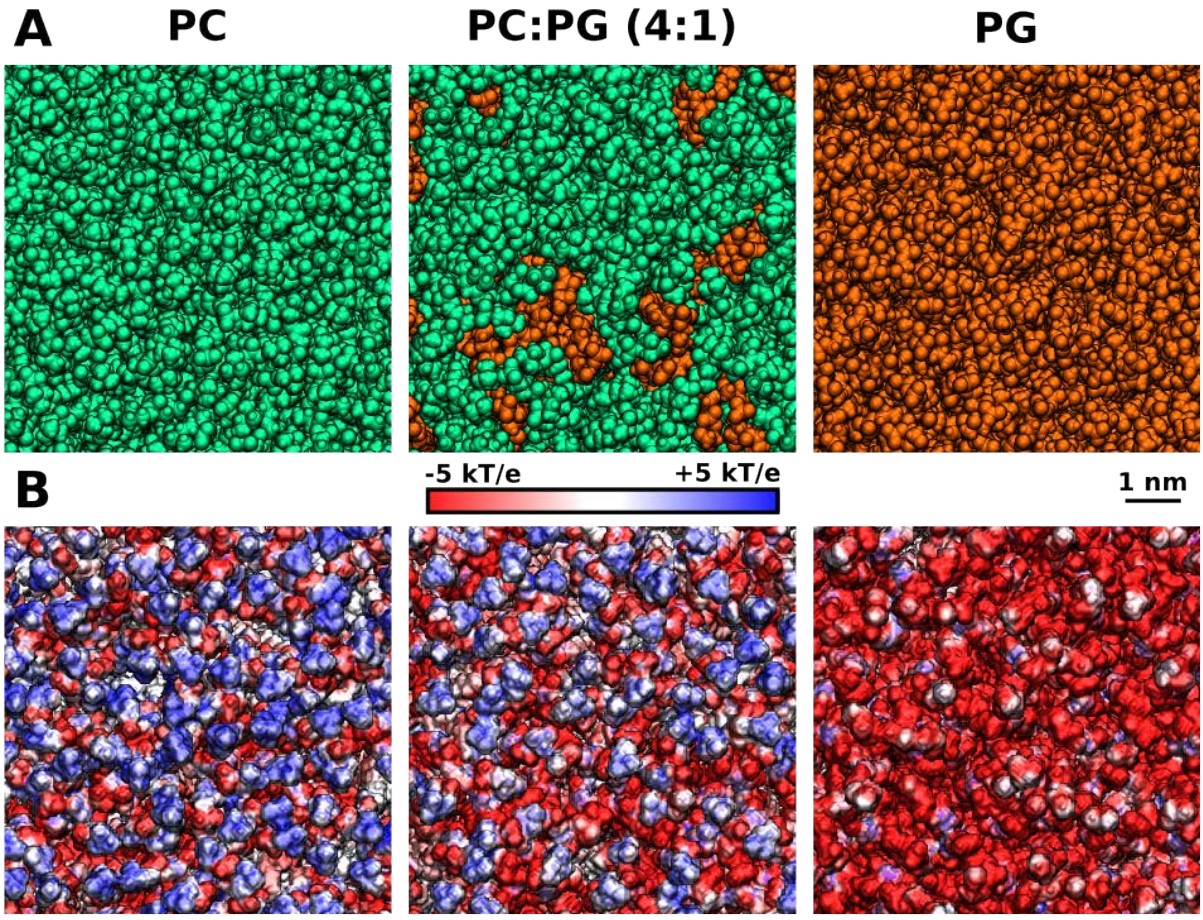

Figure S11. Phospholipid membranes simulated in this study. (A) Top views of the lipid head groups after 100 ns equilibration, with dioleoylphosphatidylcholine (PC) molecules depicted in green and dioleoylphosphatidylglycerol (PG) in orange. (B) The corresponding electrostatic potentials on the membrane surface, evaluated by means of the Poisson-Boltzmann theory in a 150 mM implicitly described monovalent salt solution. As negatively charged PG molecules are added to the membrane, the electrostatic potential becomes progressively shifted to negative values. The presence of negatively charged lipids was shown to be important for the membrane binding of several myristoylated proteins.[5-6]

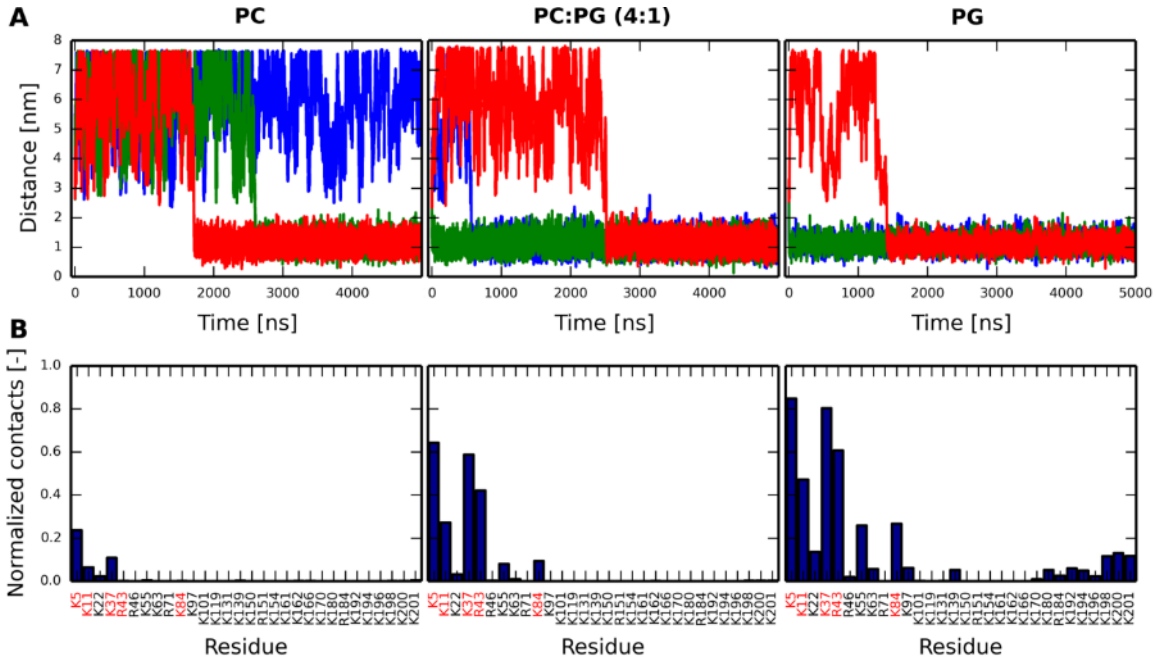

Figure S12. Membrane binding of recoverin in coarse-grained simulations with different membrane lipid compositions. (A) Distance between the center of mass of the myristoyl moiety and the central plane of the lipid bilayer in time, with different colors representing individual coarse-grained MD runs. Sudden drops to values around 1 nm mark the events of myristoyl insertion. The presence of negatively charged PG molecules in the membrane significantly accelerated the anchoring of recoverin in the membrane. (B) Relative proportion of simulation time that each basic residue of recoverin spent in contact with the membrane (distance < 0.6 nm).

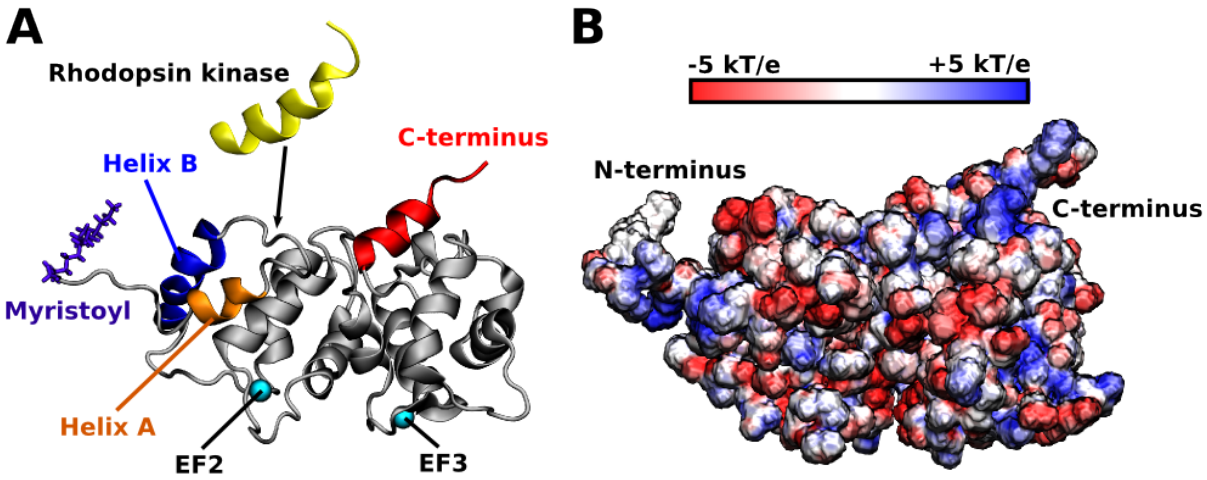

Figure S13. Structure and electrostatics of calcium-loaded recoverin. (A) Structure obtained from NMR measurements[7] (PDB ID 1JSA, structure 1). The geometry contains two calcium ions, bound in the EF2 and EF3 binding loops. The N-terminal myristoyl group is exposed to the aqueous solution as a consequence of a displacement of helices A and B, located near the N-terminus. This displacement, associated with the myristoyl switch, opens up a binding pocket for rhodopsin kinase (only an N-terminal fragment shown). The geometry of the 13 C-terminal residues (red) comes from a crystal structure[8] (PDB ID 1OMR), as it was not resolved by NMR. Overall, the protein consists of 201 amino acid residues and has a mass of 23 kDa. (B) Electrostatic potential mapped on the solvent-accessible surface of recoverin, showing patches of positively charged residues at both the N- and C-terminus. The electrostatic potential was calculated for calcium-loaded recoverin immersed in a 150 mM monovalent salt solution, treated implicitly by means of the Poisson-Boltzmann theory. The net charge of the protein is negative, equaling –3 when the charges of the two calcium ions are included.

SUPPORTING METHODS

Simulation setup for atomistic simulations

Atomistic MD simulations were performed using the GROMACS 5.1.2 package.[9] Newton's equations of motion were integrated by employing the leap-frog algorithm[10] with a time step of 2 fs. The trajectory frames were recorded every 10 ps. A cutoff of 1.2 nm was applied to short-range electrostatic interactions while long-range electrostatics was calculated with the use of the particle mesh Ewald method.[11] Van der Waals interactions were truncated at 1.2 nm; in addition, for the CHARMM force field, the van der Waals potentials were decreased so that the forces went smoothly to zero between 1.0 and 1.2 nm. Bonds with hydrogen atoms were constrained by the LINCS algorithm,[12] and water molecules were kept rigid by the SETTLE algorithm.[13] The temperature of the system was maintained at 310 K using the velocity rescaling thermostat with a stochastic term,[14] and the Parrinello–Rahman barostat[15] was utilized for semi-isotropic pressure coupling with a reference pressure of 1.01 bar. The time constants of the thermostat and barostat were 0.5 ps and 10 ps, respectively, for the AMBER force field, and 1 ps and 5 ps for the CHARMM force field.

Force field parameterization of myristoyl moiety

The simulation model for CHARMM compatible myristoyl was parameterized in two steps. In the first step force field parameters and charges for myristoyl were obtained from fatty acids section on the CHARMM-GUI website.[16] In the second step, the bond, angle, and dihedral parameters for the myristoyl–glycine connection (the amino acid to which myristoyl is attached) were obtained from the CGenFF program[17-18] at the paramchem server (https://cgenff.paramchem.org/). The obtained compatible parameters were translated to the GROMACS format using the provided cgenff_charmm2gmx.py script. For the AMBER simulations, we parameterized the myristoyl moiety with the standard AMBER atomic types, assigning partial charges to its atoms on the basis of a restrained ESP fit to a charge distribution

obtained from DFT/B3LYP calculations[19] performed for a myristamide molecule in the NWChem 6.0 software[20] using the 6-31G* basis set and the COSMO continuum solvation model[21] (see Table S3).

Table S3 (first part). Atom types and charges used for force field description of the myristoyl moiety.

	CHARMM		AMBER	
Atom name	Atom type	Charge (*e*)	Atom type	Charge (*e*)
H143	HAL3	0.090	HC	0.018400
H142	HAL3	0.090	HC	0.018400
H141	HAL3	0.090	HC	0.018400
C14	CTL3	-0.270	CT	-0.129390
H132	HAL2	0.090	HC	-0.029636
H131	HAL2	0.090	HC	-0.029636
C13	CTL2	-0.180	CT	0.173409
H122	HAL2	0.090	HC	-0.046642
H121	HAL2	0.090	HC	-0.046642
C12	CTL2	-0.180	CT	0.042167
H112	HAL2	0.090	HC	-0.037503
H111	HAL2	0.090	HC	-0.037503
C11	CTL2	-0.180	CT	0.078547
H102	HAL2	0.090	HC	-0.026833
H101	HAL2	0.090	HC	-0.026833
C10	CTL2	-0.180	CT	0.084862
H92	HAL2	0.090	HC	-0.027026
H91	HAL2	0.090	HC	-0.027026
C9	CTL2	-0.180	CT	0.058977
H82	HAL2	0.090	HC	-0.040187
H81	HAL2	0.090	HC	-0.040187

Table S3 (second part). Atom types and charges used for force field description of the myristoyl moiety.

	CHARMM		AMBER	
Atom name	Atom type	Charge (*e*)	Atom type	Charge (*e*)
C8	CTL2	-0.180	CT	0.031459
H72	HAL2	0.090	HC	-0.026583
H71	HAL2	0.090	HC	-0.026583
C7	CTL2	-0.180	CT	0.094282
H62	HAL2	0.090	HC	-0.030702
H61	HAL2	0.090	HC	-0.030702
C6	CTL2	-0.180	CT	0.051075
H52	HAL2	0.090	HC	-0.026781
H51	HAL2	0.090	HC	-0.026781
C5	CTL2	-0.180	CT	0.062140
H42	HAL2	0.090	HC	-0.026781
H41	HAL2	0.090	HC	-0.026781
C4	CTL2	-0.180	CT	0.035833
H32	HAL2	0.090	HC	-0.035143
H31	HAL2	0.090	HC	-0.035143
C3	CTL2	-0.180	CT	0.116511
H22	HAL2	0.090	HC	0.025829
H21	HAL2	0.090	HC	0.025829
C2	CTL2	-0.200	CT	-0.030802
C1	CL	0.700	C	0.547053
O1	OCL	-0.680	O	-0.615349

Force field parameters for ions and calcium-loaded EF hands

Force field parameters for calcium, chloride, and potassium ions were taken from refs.[22-23] with the electronic continuum correction applied to the ionic charges. This approach, consisting in rescaling the charge of the ion by a factor of 0.75 to account for the electronic polarizability of the surrounding water molecules, was shown to reproduce more accurately the structures of mono- and divalent salt solutions[22, 24] as well as the free energies of calcium binding to the EF hands of another calcium sensor, calmodulin.[25] In order to avoid altering the net charge of the calcium-loaded EF loops (EF2 and EF3), which could affect the recoverin–membrane interaction, we evenly distributed the excess charge of +0.5*e* among 10 (or 8) oxygen atoms potentially coordinating the calcium ion in each loop.

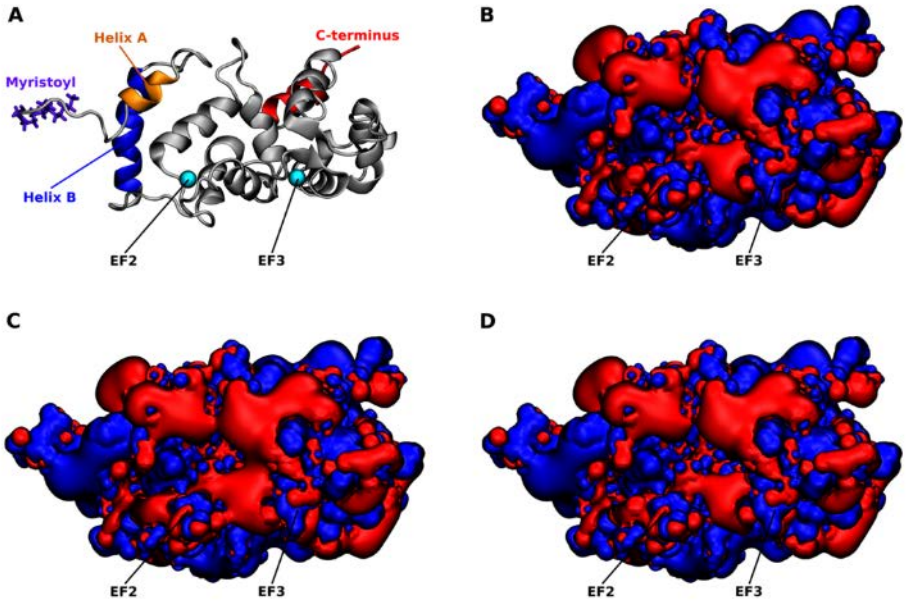

Figure S14. Effects of Ca^{2+} charge scaling and charge modifications in the EF2 and EF3 loops on the electrostatic potential around recoverin. (A) Structure of recoverin, (B) electrostatic potential around the structure with unscaled calcium charges and with protein charges obtained from the ff99SB-ILDN force field,[4] (C) electrostatic potential after rescaling the calcium charges to 1.5, featuring an enlarged negative region around the two EF loops, (D) electrostatic potential after rescaling the calcium charges and modifying charges in the two EF loops to compensate for the loss of the positive charge on each calcium. The electrostatic potentials are represented by means of positive (blue) and negative (red) isosurfaces at +2 kT/e and -2 kT/e, respectively, and were obtained using the APBS program.[26]

Protein structures and equilibration

We selected the first structure from an ensemble of 24 NMR structures of myristoylated bovine recoverin[7] (PDB code 1JSA) loaded with two Ca^{2+} ions as a starting point for our simulations. Since the last 13 C-terminal residues were not resolved by NMR measurements, we transferred the C-terminal segment (residues 185–202) from an X-ray crystal structure of non-myristoylated recoverin[8] (PDB code 1OMR). After solvation in a 150 mM aqueous KCl solution, mimicking the intracellular physiological conditions, we conducted energy minimization to ensure that the initial forces did not exceed 1000 kJ mol^{-1} nm^{-1}. This was followed by careful equilibration using two distinct equilibration protocols to obtain force-field relaxed structures of recoverin at T = 310 K and p = 1.01 bar from its initial NMR geometries. The details of these two equilibration protocols are summarized in Tables S4 and S5.

The first protocol (see Table S4) consisted of three NPT simulations, with harmonic restraints applied to all heavy atoms of the protein during the first two equilibration steps and to Cα backbone atoms only during the last step. The temperature of the system was maintained by the velocity rescaling thermostat,[14] and the pressure was controlled by the Berendsen barostat,[27] with the time constants of both the thermostat and barostat equaling 0.5 ps.

The second protocol was shorter in terms of the total simulation time but comprised twice as many equilibration steps. The first two short simulations were run in the NVT ensemble, while the following four steps were NPT simulations. Harmonic restraints were imposed on all heavy atoms of residues 10–184, excluding the ten unstructured N-terminal residues and the C-terminus. Different force constants, gradually decreasing to zero, were applied to restrain the backbone and the side chains (see Table S5). The time constants of the velocity rescaling thermostat and the Berendsen barostat were set to 1 ps.

After the three (or six, respectively) steps of each equilibration protocol, we performed a 100 ns unrestrained simulation with an integration time step of 2 fs, employing the velocity rescaling thermostat (τ = 0.5 ps) and the Parrinello–Rahman barostat (τ = 10 ps). To examine whether the stability of the N-terminus depended on the choice of a particular structure from the NMR ensemble, we repeated the

equilibrations also for the eighth structure of the ensemble, differing the most from the first structure in terms of the root-mean-square deviation (RMSD) of the N-terminus. The resulting relaxed structures of recoverin for the different force fields, initial geometries, and equilibration protocols are characterized in Table S6 and Figure S7.

Table S4. Summary of equilibration protocol 1. The letter *k* denotes the force constant of the harmonic restraints.

Step	Length [ns]	Time step [fs]	Restraints	k [kJ mol^{-1} nm^{-2}]
1	0.1	1	heavy atoms, all residues	1000
2	1	2	heavy atoms, all residues	1000
3	25	2	Cα, all residues	1000

Table S5. Summary of equilibration protocol 2. Harmonic restraint potentials with different force constants ($k_{backbone}$ and $k_{sidechain}$) were applied to the backbone and side chain atoms.

Step	Length [ns]	Time step [fs]	Restraints	$k_{backbone}$ [kJ mol^{-1} nm^{-2}]	$k_{sidechain}$ [kJ mol^{-1} nm^{-2}]
1	0.1	1	heavy atoms, residues 10─184	1000	500
2	0.1	1	heavy atoms, residues 10─184	500	250
3	0.1	1	heavy atoms, residues 10─184	250	100
4	0.5	2	heavy atoms, residues 10─184	100	50
5	0.5	2	heavy atoms, residues 10─184	50	0
6	0.5	2	none	0	0

Table S6. Relaxed structures obtained with different force fields, initial NMR geometries[7] (taken from PDB ID 1JSA), and different equilibration protocols.

Force field	NMR structure	Equilibration protocol	Myristoyl	Helices	RMSD from initial structure [Å]
CHARMM	**1**	**1**	**Exposed**	**Helix A remains helical.**	**3.1**
CHARMM	1	2	Hidden	Helix A prolonged, becomes parallel with B	4.9
CHARMM	8	1	Hidden	Helix A prolonged, becomes parallel with B.	4.2
CHARMM	8	2	Hidden	Helix A prolonged, becomes parallel with B.	4.6
AMBER	1	1	Hidden	Helix A loses structure.	4.9
AMBER	1	2	Hidden	Helix A remains helical but moves.	4.4
AMBER	8	1	Hidden	Helix A loses structure, helix B moves.	4.4
AMBER	**8**	**2**	**Exposed**	**Helix A remains helical but changes angle to helix B.**	**3.8**

Structure of recoverin binding rhodopsin kinase

A set of recoverin structures binding an N-terminal fragment (the first 25 residues) of rhodopsin kinase (RK) was previously determined from NMR measurements[28] (PDB code 2I94). However, since the RK-binding NMR structure of recoverin lacked the myristoyl moiety and its first six N-terminal residues were not located by the experiments, we did not use the 2I94 structure directly as an initial geometry in our simulation, but, by performing a targeted MD simulation and taking the RK-binding 2I94 structure[28] as a reference, we accommodated the RK fragment in the binding pocket of the previously described RK-free 1JSA structure.[7] To avoid placing charge on the C-terminal end of the 16 residue RK segment resolved by NMR, we capped it with a methyl group. The targeted MD was performed in GROMACS 5.1.2[9] patched with the Plumed 2.2.3 package.[29] First, structures of an RK-free recoverin[7] (PDB 1JSA, structure 1) and an N-terminal fragment of RK[8] (from PDB 2I94, structure 1) were together solvated in a

150 mM KCl aqueous solution so that the RK fragment was initially not in contact with recoverin. Then, after energy minimization and a quick equilibration run identical with the first step of equilibration protocol 1, we performed a 20 ns targeted MD simulation, gradually lowering the Cα RMSD of the system with respect to the first structure of PDB 2I94 until the RMSD reached values below 0.25 nm. This resulted in binding of RK to recoverin accompanied by widening of the binding pocket, in agreement with the 2I94 structure. The force constant used for the targeted MD run was 5000 kJ mol^{-1} nm^{-2}.

Membrane building and equilibration

The phospholipid bilayers were assembled and hydrated with the use of the CHARMM-GUI membrane builder.[16, 30-31] A minimization and equilibration protocol[32] provided by CHARMM-GUI was subsequently employed to relax each membrane. Before adding recoverin to the membrane, we performed a 100 ns simulation to further equilibrate the bilayer.

Umbrella sampling of membrane insertion of myristamide

All-atom umbrella sampling (US) of the insertion of a myristamide molecule into a PC:PG (4:1) bilayer was performed using the GROMACS 5.1.2 package.[9] The simulations were repeated with both the CHARMM and AMBER force field, and the simulation settings were consistent with our simulations of the recoverin–membrane system described with the respective force field (see above). The force field description of myristamide was based on the parameterization of the myristoyl moiety in the recoverin–membrane simulations (see above), with bonded and van der Waals parameters for the amide group assigned by the GROMACS pdb2gmx tool using the parameters for an amidated protein C-terminus (residues CT2 and NH2 in CHARMM and AMBER, respectively). The atomic charges for the amide group (Table S7) were adopted from the amidated protein C-terminus (CHARMM) or obtained from a RESP fit (AMBER, see *Force field parameterization of myristoyl moiety*). The simulation box contained a PC:PG (4:1) bilayer consisting of 104 PC lipids and 26 PG lipids, 150 mM KCl, including additional K^+ ions to neutralize the negative charge of the membrane**,** ~7700 water molecules**,** and one myristamide

molecule. The lipid bilayer was assembled and solvated by employing the CHARMM-GUI server.[16, 30-31] Prior to insertion of the myristamide to the simulation box, a 50 ns unrestrained NPT simulation following the standard minimization and equilibration protocol provided by CHARMM-GUI[32] was used to equilibrate the bilayer. For the AMBER (Slipids) force field, the initial minimization step was performed without any bond constraints imposed on the lipid molecules to allow for better adjustment of the CHARMM-GUI generated lipid geometries to the Slipids model. As the reaction coordinate for our umbrella sampling simulations, the distance between the center of mass (COM) of the myristamide molecule and the central plane of the bilayer was used. The umbrella windows were placed along the reaction coordinate with a spacing of ~0.1 nm, resulting in a total of ~35 umbrella windows for each set of US simulations. The initial geometries for the individual umbrella windows were generated by performing two unrestrained 50 ns simulations. In both simulations, the myristamide molecule was initially placed in the bulk solution, without any contact with the bilayer. Since myristamide moved to the inside of the membrane in all of these trajectories, we were able to extract the starting geometries from the course of these membrane insertion events. In addition, to check the convergence of the free energy profile for the AMBER system, we used two pulling protocols to generate the starting geometries: In the first pulling protocol, membrane-embedded myristamide (geometry taken from the spontaneous insertion) was pulled out to the solution, while in the second protocol, the myristamide molecule was pulled into the membrane from the solution. In the case of pulling myristamide out, the molecule was pulled for 1 ns along the z-axis, using a spring constant of 100 kJ mol^{-1} nm^{-2} and a pull rate of 0.005 nm ps^{-1}. In the other case, myristamide was pulled inside the membrane for 2 ns along the z-axis, using the same spring constant and pulling rate as before. Myristamide COM distance from the central plane of the bilayer was used as the pull coordinate when pulling the molecule out, while the distance of its methyl carbon was used for pulling it in the other direction. After generating the initial structures, a 100 ps NPT equilibration was performed for each umbrella window before the actual US simulation. This equilibration was followed by 10 ns of production US simulation using a harmonic potential with a force constant of 1000 kJ mol^{-1} nm^{-2}. To ensure convergence of umbrella windows located near the membrane–water interface,

where the myristamide tail was oscillating between being solvent-exposed and partially buried in the bilayer, we extended several of these windows to 50 ns. This concerned eight umbrella windows between 2.23 and 2.90 nm for the CHARMM system, four umbrella windows between 2.15 and 2.78 nm in the set of AMBER umbrella simulations with initial geometries from spontaneous insertion, four umbrella windows between 2.21 and 2.66 nm in the AMBER "pulling out" set, and six simulations between 2.17 and 2.76 nm in the AMBER "pulling in" set. We then employed the weighted histogram analysis (WHAM) method[33] to obtain the free energy profiles, using the bootstrap analysis method[34] for estimating statistical errors.

Table S7. Atom types and charges used for force field description of the amide group in myristamide. The atomic charges assigned to the remaining atoms of myristamide were identical to those used for the myristoyl moiety (Table S3), with the exception of the charge on atom C2 in CHARMM, which was adjusted by +0.020*e* to maintain electroneutrality of the whole residue.

	CHARMM		AMBER	
Atom name	Atom type	Charge (*e*)	Atom type	Charge (*e*)
C1	CC	0.550	C	0.547053
O1	O	-0.550	O	-0.615349
N	NH2	-0.620	N	-0.719478
H1	H	0.300	H	0.345247
H2	H	0.320	H	0.374231

Umbrella sampling of membrane interaction of non-myristoylated recoverin

Umbrella sampling (US) of the binding of a non-myristoylated recoverin to a PC:PG (4:1) bilayer was done in the GROMACS 5.1.2 program.[9] The simulations utilized the CHARMM force field, and the simulation settings were consistent with the atomistic trajectories of the recoverin–membrane system (see above). The distance between the center of mass (COM) of the protein and the central plane of the bilayer was used as the reaction coordinate. A total of 24 umbrella windows were placed along the reaction coordinate, covering a range between 4.0 and 7.0 nm. The initial geometries for the nine lowest umbrella

windows were obtained from a MD simulation of non-myristoylated recoverin (Table S1, run 22) capturing its detachment from the membrane. The initial geometries of the remaining 15 umbrella windows were generated by using a pull protocol along the reaction coordinate with a force constant of 100 kJ mol^{-1} nm^{-2} and a pull rate of 0.0005 nm ps^{-1}. For the four highest umbrella windows, the z-dimension of the simulation box was increased by adding extra ~4000 water molecules to the system to ensure that the value of the reaction coordinate did not exceed one half of the box height during the US simulations. Each umbrella window was then simulated for 50 ns using a harmonic potential with a force constant of 1000 kJ mol^{-1} nm^{-2}. The free energy profiles were obtained by employing the weighted histogram analysis (WHAM) method[33], and the bootstrap analysis method[34] was used for estimating statistical errors.

Coarse-grained MD simulations

The coarse-grained simulations presented in this article utilized the MARTINI model.[35] A structure of recoverin (based on PDB 1JSA 1) which was obtained with the AMBER force field after equilibration with restrained Cα carbons (see *Protein structures and equilibration* and the first equilibration protocol) was mapped into the MARTINI coarse-grained representation using the martinize.py script.[36] The ELNEDYN representation[37] with r_c 0.9 nm and f_c 500 kJ mol^{-1} nm^{-2} excluding the first nine residues (2 to 10) was used to prevent any undesired large conformational changes during coarse-grained MD simulations. Parameters for N-myristoylated glycine were taken from Charlier et al.[38] MARTINI coarse-grained models of dioleoylphosphatidylcholine (PC) and dioleoylphosphatidylglycerol (PG) were taken from Refs. [36, 39]. Lipid bilayers, in total composed of 256 lipid molecules with different amounts of PC and PG were prepared utilizing the insane.py script.[40] All coarse-grained MD simulations were done in GROMACS 4.6.5.[41] Lennard–Jones and electrostatic interactions were shifted to 0 between 0.9 and 1.2 nm and between 0 and 1.2 nm, respectively. A relative dielectric constant of 15 was used. The simulations were run in the NPT ensemble. The temperature of protein, lipids, and the solvent was coupled separately at 310 K using the Berendsen thermostat,[27] with a coupling constant of 1.0 ps. The

system pressure was coupled using the Berendsen barostat[27] with a coupling constant of 3.0 ps, a compressibility of 3.0, and a reference pressure of 1 bar. The simulations were performed using a 20 fs integration time step. Initially, the protein was placed 2.0 nm apart the membrane. Subsequently, we solvated the system in the standard MARTINI water containing 150 mM NaCl. Extra Na^+ ions were added to the solution to ensure electroneutrality of the system. The whole system was energy minimized using the steepest descent method up to a maximum of 500 steps and production runs were performed for 5 μs. It is important to note that the times reported in this study are computational times. It was shown that effective times for coarse-grained MD simulations are longer; for proteins and lipids in the MARTINI force field, the scaling factor is about fourfold, that is, 5 μs of simulation time would correspond to 20 μs of real time.[42] Standard GROMACS tools as well as in-house codes were used for analysis.

In addition to standard MARTINI simulations, we obtained additional trajectories with a PC:PG (4:1) bilayer by employing the polarizable version of the MARTINI force field.[43] The system was prepared in the same way as those in the standard non-polarizable MARTINI simulations. Importantly, long-range electrostatics was treated using the particle mesh Ewald method[11] while short-range electrostatic interactions were truncated at 1.2 nm. In addition, a relative dielectric constant of 2.5 was employed instead of 15.

Electrostatics calculations

Electrostatic potentials in the vicinity of both recoverin and the bilayers immersed in a 150 mM monovalent salt solution were calculated by numerically solving the nonlinear Poisson-Boltzmann equation in the APBS program.[26] A sequence of two focusing steps was performed with both the coarse and the fine grid centered on the protein/membrane. The dimensions of the two grids, consisting of 193 grid points along each dimension, were 30 nm x 30 nm x 30 nm and 10 nm x 10 nm x 10 nm, respectively. The interior of the protein/membrane was modeled as a dielectric with a relative permittivity of 2, while the aqueous environment surrounding the protein/membrane was assigned a relative

permittivity of 78.54. The molecular surface of the protein/membrane was constructed as their van der Waals surface.

SUPPORTING RESULTS

Coarse-grained MD simulations with the polarizable MARTINI force field

We performed additional coarse-grained simulations of recoverin in the proximity of a PC:PG (4:1) bilayer using the polarizable MARTINI force field (see Table S2). In all three trajectories, we observed membrane insertion of the myristoyl moiety, which is consistent with the standard non-polarizable MARTINI simulations. After the successful membrane anchoring, the N-terminal domain was positioned close to the membrane while the C-terminal domain was located farther away, which is in qualitative agreement with the non-polarizable simulations. While recoverin also sampled the tilted orientation observed in the corresponding non-polarizable MARTINI simulations, we found that the dominant orientation became more upright (see Fig. S15A) and that the five positively charged residues K5, K11, K37, R43, and K84 identified by NMR interacted less strongly with the membrane (Fig. S15B). Thus, we observed that the stabilizing effect of the positively charged protein residues near the N-terminus, promoting the tilted orientation of recoverin, while being still present, was partially attenuated by an enhanced screening of the electrostatic interactions, pertinent to the polarizable MARTINI force field. A similar weakened interaction with a charged membrane in a polarizable MARTINI simulation was also reported for the HIV-1 matrix protein.[38]

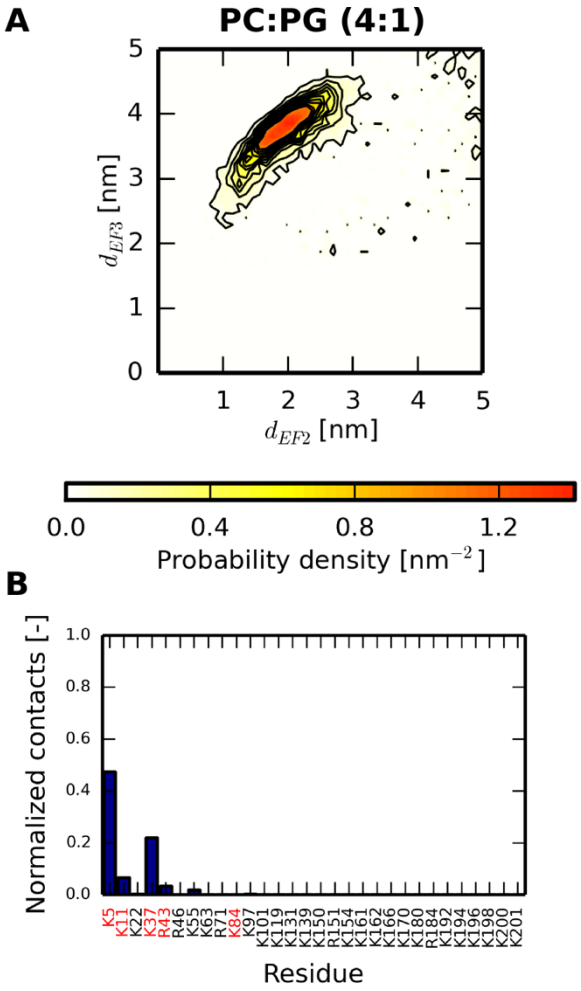

Figure S15. Combined results of three 2.5 μs coarse-grained MD trajectories using the polarizable MARTINI model (see Table S2) with a PC:PG (4:1) bilayer. **(**A) Membrane orientation of recoverin toward the lipid bilayer. The plot represents the probability density of the distances of the two calcium ions from the membrane. (B) Relative proportion of simulation time that each basic residue of recoverin spent in contact with the membrane (distance < 0.6 nm).

SUPPORTING REFERENCES

1. Valentine, K. G.; Mesleh, M. F.; Opella, S. J.; Ikura, M.; Ames, J. B., Structure, topology, and dynamics of myristoylated recoverin bound to phospholipid bilayers. *Biochemistry* **2003,** *42* (21), 6333-6340.
2. MacKerell, A. D.; Bashford, D.; Bellott, M.; Dunbrack, R. L.; Evanseck, J. D.; Field, M. J.; Fischer, S.; Gao, J.; Guo, H.; Ha, S.; Joseph-McCarthy, D.; Kuchnir, L.; Kuczera, K.; Lau, F. T. K.; Mattos, C.; Michnick, S.; Ngo, T.; Nguyen, D. T.; Prodhom, B.; Reiher, W. E.; Roux, B.; Schlenkrich, M.; Smith, J. C.; Stote, R.; Straub, J.; Watanabe, M.; Wiorkiewicz-Kuczera, J.; Yin, D.; Karplus, M., All-atom empirical potential for molecular modeling and dynamics studies of proteins. *J. Phys. Chem. B* **1998,** *102* (18), 3586-3616.
3. MacKerell, A. D.; Feig, M.; Brooks, C. L., Extending the treatment of backbone energetics in protein force fields: Limitations of gas-phase quantum mechanics in reproducing protein conformational distributions in molecular dynamics simulations. *J. Comput. Chem.* **2004,** *25* (11), 1400-1415.
4. Lindorff-Larsen, K.; Piana, S.; Palmo, K.; Maragakis, P.; Klepeis, J. L.; Dror, R. O.; Shaw, D. E., Improved side-chain torsion potentials for the Amber ff99SB protein force field. *Proteins: Struct. Funct. Bioinform.* **2010,** *78* (8), 1950-1958.
5. Murray, D.; Ben-Tal, N.; Honig, B.; McLaughlin, S., Electrostatic interaction of myristoylated proteins with membranes: simple physics, complicated biology. *Structure* **1997,** *5* (8), 985-989.
6. Mulgrew-Nesbitt, A.; Diraviyam, K.; Wang, J.; Singh, S.; Murray, P.; Li, Z.; Rogers, L.; Mirkovic, N.; Murray, D., The role of electrostatics in protein-membrane interactions. *Biochim. Biophys. Acta, Mol. Cell. Biol. Lipids* **2006,** *1761* (8), 812-826.
7. Ames, J. B.; Ishima, R.; Tanaka, T., Molecular mechanics of calcium–myristoyl switches. *Nature* **1997,** *389* (6647), 198-202.
8. Weiergraber, O. H.; Senin, I. I.; Philippov, P. P.; Granzin, J.; Koch, K. W., Impact of N-terminal myristoylation on the Ca^{2+}-dependent conformational transition in recoverin. *J. Biol. Chem.* **2003,** *278* (25), 22972-22979.
9. Abraham, M. J.; Murtola, T.; Schulz, R.; Páll, S.; Smith, J. C.; Hess, B.; Lindahl, E., GROMACS: High performance molecular simulations through multi-level parallelism from laptops to supercomputers. *SoftwareX* **2015,** *1–2*, 19-25.
10. Hockney, R. W.; Goel, S. P.; Eastwood, J. W., Quiet High-Resolution Computer Models of a Plasma. *Journal of Computational Physics* **1974,** *14* (2), 148-158.
11. Darden, T.; York, D.; Pedersen, L., Particle Mesh Ewald - an N.Log(N) Method for Ewald Sums in Large Systems. *J. Chem. Phys.* **1993,** *98* (12), 10089-10092.
12. Hess, B.; Bekker, H.; Berendsen, H. J. C.; Fraaije, J., LINCS: A linear constraint solver for molecular simulations. *J. Comput. Chem.* **1997,** *18* (12), 1463-1472.
13. Miyamoto, S.; Kollman, P. A., Settle - an Analytical Version of the Shake and Rattle Algorithm for Rigid Water Models. *J. Comput. Chem.* **1992,** *13* (8), 952-962.
14. Bussi, G.; Donadio, D.; Parrinello, M., Canonical sampling through velocity rescaling. *J. Chem. Phys.* **2007,** *126* (1), 014101.
15. Parrinello, M.; Rahman, A., Polymorphic Transitions in Single-Crystals - a New Molecular-Dynamics Method. *J. Appl. Phys.* **1981,** *52* (12), 7182-7190.
16. Jo, S.; Kim, T.; Iyer, V. G.; Im, W., Software news and updates - CHARMM-GUI: A web-based graphical user interface for CHARMM. *J. Comput. Chem.* **2008,** *29* (11), 1859-1865.
17. Vanommeslaeghe, K.; MacKerell, A. D., Automation of the CHARMM General Force Field (CGenFF) I: Bond Perception and Atom Typing. *J. Chem. Inf. Model.* **2012,** *52* (12), 3144-3154.
18. Vanommeslaeghe, K.; Raman, E. P.; MacKerell, A. D., Automation of the CHARMM General Force Field (CGenFF) II: Assignment of Bonded Parameters and Partial Atomic Charges. *J. Chem. Inf. Model.* **2012,** *52* (12), 3155-3168.
19. Becke, A. D., Density-Functional Thermochemistry. III. The Role of Exact Exchange. *J. Chem. Phys.* **1993,** *98* (7), 5648-5652.

20. Valiev, M.; Bylaska, E. J.; Govind, N.; Kowalski, K.; Straatsma, T. P.; Van Dam, H. J. J.; Wang, D.; Nieplocha, J.; Apra, E.; Windus, T. L.; de Jong, W., NWChem: A comprehensive and scalable open-source solution for large scale molecular simulations. *Comput. Phys. Commun.* **2010,** *181* (9), 1477-1489.
21. Klamt, A.; Schuurmann, G., COSMO: A new approach to dielectric screening in solvents with explicit expressions for the screening energy and its gradient. *J. Chem. Soc., Perkin Trans. 2* **1993,** (5), 799-805.
22. Kohagen, M.; Mason, P. E.; Jungwirth, P., Accurate Description of Calcium Solvation in Concentrated Aqueous Solutions. *J. Phys. Chem. B* **2014,** *118* (28), 7902-7909.
23. Chang, T. M.; Dang, L. X., Detailed study of potassium solvation using molecular dynamics techniques. *J. Phys. Chem. B* **1999,** *103* (22), 4714-4720.
24. Kohagen, M.; Pluharova, E.; Mason, P. E.; Jungwirth, P., Exploring Ion-Ion Interactions in Aqueous Solutions by a Combination of Molecular Dynamics and Neutron Scattering. *J. Phys. Chem. Lett.* **2015,** *6* (9), 1563-1567.
25. Kohagen, M.; Lepsik, M.; Jungwirth, P., Calcium Binding to Calmodulin by Molecular Dynamics with Effective Polarization. *J. Phys. Chem. Lett.* **2014,** *5* (22), 3964-3969.
26. Baker, N. A.; Sept, D.; Joseph, S.; Holst, M. J.; McCammon, J. A., Electrostatics of nanosystems: Application to microtubules and the ribosome. *Proc. Natl. Acad. Sci. USA* **2001,** *98* (18), 10037-10041.
27. Berendsen, H. J. C.; Postma, J. P. M.; Vangunsteren, W. F.; Dinola, A.; Haak, J. R., Molecular dynamics with coupling to an external bath. *J. Chem. Phys.* **1984,** *81* (8), 3684-3690.
28. Ames, J. B.; Levay, K.; Wingard, J. N.; Lusin, J. D.; Slepak, V. Z., Structural basis for calcium-induced inhibition of rhodopsin kinase by recoverin. *J. Biol. Chem.* **2006,** *281* (48), 37237-37245.
29. Tribello, G. A.; Bonomi, M.; Branduardi, D.; Camilloni, C.; Bussi, G., PLUMED 2: New feathers for an old bird. *Comput. Phys. Commun.* **2014,** *185* (2), 604-613.
30. Jo, S.; Lim, J. B.; Klauda, J. B.; Im, W., CHARMM-GUI Membrane Builder for Mixed Bilayers and Its Application to Yeast Membranes. *Biophys. J.* **2009,** *97* (1), 50-58.
31. Wu, E. L.; Cheng, X.; Jo, S.; Rui, H.; Song, K. C.; Davila-Contreras, E. M.; Qi, Y. F.; Lee, J. M.; Monje-Galvan, V.; Venable, R. M.; Klauda, J. B.; Im, W., CHARMM-GUI Membrane Builder Toward Realistic Biological Membrane Simulations. *J. Comput. Chem.* **2014,** *35* (27), 1997-2004.
32. Lee, J.; Cheng, X.; Swails, J. M.; Yeom, M. S.; Eastman, P. K.; Lemkul, J. A.; Wei, S.; Buckner, J.; Jeong, J. C.; Qi, Y. F.; Jo, S.; Pande, V. S.; Case, D. A.; Brooks, C. L.; MacKerell, A. D.; Klauda, J. B.; Im, W., CHARMM-GUI Input Generator for NAMD, GROMACS, AMBER, OpenMM, and CHARMM/OpenMM Simulations Using the CHARMM36 Additive Force Field. *J. Chem. Theory Comput.* **2016,** *12* (1), 405-413.
33. Kumar, S.; Bouzida, D.; Swendsen, R. H.; Kollman, P. A.; Rosenberg, J. M., The Weighted Histogram Analysis Method for Free-Energy Calculations on Biomolecules. 1. The Method. *J. Comput. Chem.* **1992,** *13* (8), 1011-1021.
34. Hub, J. S.; de Groot, B. L.; van der Spoel, D., g_wham-A Free Weighted Histogram Analysis Implementation Including Robust Error and Autocorrelation Estimates. *J. Chem. Theory Comput.* **2010,** *6* (12), 3713-3720.
35. Monticelli, L.; Kandasamy, S. K.; Periole, X.; Larson, R. G.; Tieleman, D. P.; Marrink, S. J., The MARTINI coarse-grained force field: Extension to proteins. *J. Chem. Theory Comput.* **2008,** *4* (5), 819-834.
36. de Jong, D. H.; Singh, G.; Bennett, W. F. D.; Arnarez, C.; Wassenaar, T. A.; Schafer, L. V.; Periole, X.; Tieleman, D. P.; Marrink, S. J., Improved Parameters for the Martini Coarse-Grained Protein Force Field. *J. Chem. Theory Comput.* **2013,** *9* (1), 687-697.
37. Periole, X.; Cavalli, M.; Marrink, S. J.; Ceruso, M. A., Combining an Elastic Network With a Coarse-Grained Molecular Force Field: Structure, Dynamics, and Intermolecular Recognition. *J. Chem. Theory Comput.* **2009,** *5* (9), 2531-2543.
38. Charlier, L.; Louet, M.; Chaloin, L.; Fuchs, P.; Martinez, J.; Muriaux, D.; Favard, C.; Floquet, N., Coarse-Grained Simulations of the HIV-1 Matrix Protein Anchoring: Revisiting Its Assembly on Membrane Domains. *Biophys. J.* **2014,** *106* (3), 577-585.

39. Ingolfsson, H. I.; Melo, M. N.; van Eerden, F. J.; Arnarez, C.; Lopez, C. A.; Wassenaar, T. A.; Periole, X.; de Vries, A. H.; Tieleman, D. P.; Marrink, S. J., Lipid Organization of the Plasma Membrane. *J. Am. Chem. Soc.* **2014,** *136* (41), 14554-14559.
40. Wassenaar, T. A.; Ingolfsson, H. I.; Bockmann, R. A.; Tieleman, D. P.; Marrink, S. J., Computational Lipidomics with insane: A Versatile Tool for Generating Custom Membranes for Molecular Simulations. *J. Chem. Theory Comput.* **2015,** *11* (5), 2144-2155.
41. Hess, B.; Kutzner, C.; van der Spoel, D.; Lindahl, E., GROMACS 4: Algorithms for highly efficient, load-balanced, and scalable molecular simulation. *J. Chem. Theory Comput.* **2008,** *4* (3), 435-447.
42. Marrink, S. J.; Tieleman, D. P., Perspective on the Martini model. *Chem. Soc. Rev.* **2013,** *42* (16), 6801-6822.
43. Yesylevskyy, S. O.; Schafer, L. V.; Sengupta, D.; Marrink, S. J., Polarizable Water Model for the Coarse-Grained MARTINI Force Field. *PLoS Comp. Biol.* **2010,** *6* (6), e1000810.